Inorg. Chem. **2004**, *43*, 7210–7217

A Platinum–Ruthenium Dinuclear Complex Bridged by Bis(terpyridyl)xanthene

Rei Okamura, Tohru Wada, Katsuji Aikawa, Toshi Nagata, and Koji Tanaka*

Institute for Molecular Science and CREST, Japan Science and Technology Agency(JST), Higashiyama 5-1, Myodaiji, Okazaki, Aichi 444-8787, Japan

Received March 12, 2004

4,5-Bis(terpyridyl)-2,7-di-*tert*-butyl-9,9-dimethylxanthene (btpyxa) was prepared to serve as a new bridging ligand via Suzuki coupling of terpyridin-4′-yl triflate and 2,7-di-*tert*-butyl-9,9-dimethylxanthene-4,5-diboronic acid. The reaction of btpyxa with either 1 equiv or an excess of $PtCl_2$(cod) (cod = 1,5-cyclooctadiene) followed by anion exchange afforded mono- and dinuclear platinum complexes [(PtCl)(btpyxa)](PF_6) ([**1**](PF_6)) and [$(PtCl)_2$(btpyxa)]$(PF_6)_2$ ([**2**]-$(PF_6)_2$), respectively. The X-ray crystallography of [**1**]$(PF_6)\cdot CHCl_3$ revealed that the two terpyridine units in the ligand are nearly parallel to each other. The heterodinuclear complex [(PtCl){Ru(^{t}Bu$_2$SQ)(dmso)}(btpyxa)]$(PF_6)_2$ ([**4**]$(PF_6)_2$) (dmso = dimethyl sulfoxide; ^{t}Bu$_2$SQ = 3,5-di-*tert*-butyl-1,2-benzosemiquinone) and the monoruthenium complex [Ru(^{t}Bu$_2$SQ)(dmso)(trpy)](PF_6) ([**5**](PF_6)) (trpy = 2,2′:6′,2″-terpyridine) were also synthesized. The CV of [**2**]$^{2+}$ suggests possible electronic interaction between the two Pt(trpy) groups, whereas such an electronic interaction was not suggested by the CV of [**4**]$^{2+}$ between Pt(trpy) and Ru(^{t}Bu$_2$SQ) frameworks.

Introduction

Metal−dioxolene complexes undergo not only metal-centered redox reactions but also ligand-based ones, since dioxolene ligands can exist in quinone, semiquinone, and catecholato forms depending on oxidation state.[1] Ruthenium−dioxolene complexes are particularly interesting in this regard by virtue of the closeness of energy levels for the 4d orbitals of ruthenium and the π^* orbitals of the ligand. Such delocalization (charge distribution) of π electrons over the Ru−dioxolene frameworks sometimes results in unusual electronic structures.[2,3] Recently, we demonstrated that deprotonation of an aquo ligand in Ru−dioxolene complexes caused intramolecular electron transfer from the resultant hydroxy or oxo group to the Ru−dioxolene framework to form unprecedented hydroxyl (or oxyl) radical complexes.[4] The similar conversion from two aquo to two oxo ligands in a bis(ruthenium−dioxolene) complex enabled the catalytic four-electron oxidation of water at pH 4.0.[5] Furthermore, oxyl radical complexes are proven to have the ability to oxidize certain organic molecules.[6] Heterodinuclear complexes having a Ru−dioxolene−aquo framework, therefore, may provide unique reaction sites for organic molecules if the second metal site traps those organic substrates. Accordingly, we have designed a new binding ligand, 4,5-bis(terpyridyl)-2,7-di-*tert*-butyl-9,9-dimethylxanthene (btpyxa) in which the 4′-positions of two terpyridines are linked at the 4- and 5-positions of the xanthene skeleton, which is capable of fixing two metal terpyridyl complexes at the same site.

Experimental Section

Materials. Commercially available $PtCl_2$, K_2PtCl_4, $RuCl_3$, ethyl picolinate, 4,5-dibromo-2,7-di-*tert*-butyl-9,9-dimethylxanthene, 2,2′:6′,2″-terpyridine, and $Pd(PPh_3)_4$ were used without further purifica-

* Author to whom correspondence should be addressed. E-mail: ktanaka@ims.ac.jp.

(1) (a) Pierpont, C. G.; Buchanan, R. M. *Coord. Chem. Rev.* **1981**, *38*, 45−87. (b) Pierpont, C. G.; Lange, C. W. *Prog. Inorg. Chem.* **1994**, *41*, 331−442. (c) Pierpont, C. G. *Coord. Chem. Rev.* **2001**, *216*−*217*, 99−125.

(2) (a) Haga, M.; Dodsworth, E. S.; Lever, A. B. P.; Boone, S. R.; Pierpont, C. G. *J. Am. Chem. Soc.* **1986**, *108*, 7413−7414. (b) Boone, S. R.; Pierpont, C. G. *Inorg. Chem.* **1987**, *26*, 1769−1773. (c) Bhattacharya, S.; Pierpont, C. G. *Inorg. Chem.* **1991**, *30*, 1511−1516. (d) Bhattacharya, S.; Boone, S. R.; Fox, G. A.; Pierpont, C. G. *J. Am. Chem. Soc.* **1990**, *112*, 1088−1096. (e) Bhattacharya, S.; Pierpont, C. G. *Inorg. Chem.* **1994**, *33*, 6038−6042.

(3) (a) Haga, M.; Dodsworth, E. S.; Lever, A. B. P. *Inorg. Chem.* **1986**, *25*, 447−453. (b) Lever, A. P. B.; Auburn, P. R.; Dodsworth, E. S.; Haga, M.; Liu, W.; Melnik, M.; Nevin, W. A. *J. Am. Chem. Soc.* **1988**, *110*, 8076−8084. (c) Masui, H.; Lever, A. B. P.; Auburn, P. R. *Inorg. Chem.* **1991**, *30*, 2402−2410. (d) Auburn, P. R.; Dodsworth, E. S.; Haga, M.; Liu, W.; Nevin, W. A.; Lever, A. P. B. *Inorg. Chem.* **1991**, *30*, 3502−3512.

(4) Kobayashi, K.; Ohtsu, H.; Wada. T.; Kato, T.; Tanaka, K. *J. Am. Chem. Soc.* **2003**, *125*, 6729−6739.

(5) (a) Wada, T.; Tsuge, K.; Tanaka, K. *Angew. Chem., Int. Ed.* **2000**, *39*, 1479−1482. (b) Wada, T.; Tsuge, K.; Tanaka, K. *Inorg. Chem.* **2001**, *40*, 329−337.

(6) Wada, T.; Tsuge, K.; Tanaka, K. *Chem. Lett.* **2000**, 910−911.

10.1021/ic049680n CCC: $27.50
Published on Web 10/01/2004

tion. The tetrabutylammonium hexafluorophosphate used as a supporting electrolyte for electrochemistry was recrystallized from hot ethanol. 4′-{(Trifluoromethanesulfonyl)oxy}-2,2′:6′,2″-terpyridine,[7] 2,7-di-*tert*-butyl-9,9-dimethylxanthene-4,5-diboronic acid,[8] $PtCl_2(PhCN)_2$,[9] $PtCl_2$(cod),[10] $RuCl_2$(dmso)$_4$,[11] and $RuCl_2$(dmso)(trpy)[12] were prepared according to the literature.

Syntheses of the Ligand and the Complexes. 4,5-Bis(terpyridyl)-2,7-di-*tert*-butyl-9,9-dimethylxanthene (btpyxa). A mixture of 2,7-di-*tert*-butyl-9,9-dimethylxanthene-4,5-diboronic acid (1.01 g, 2.47 mmol), 4′-{(trifluoromethanesulfonyl)oxy}-2,2′:6′,2″-terpyridine (1.89 g, 4.94 mmol), $Pd(PPh_3)_4$ (205 mg, 0.177 mmol), and Na_2CO_3 (1.05 g, 9.89 mmol) was stirred in DMF (50 mL) at 110 °C overnight under N_2. After the solvent was evaporated in vacuo, the residue was extracted with CH_2Cl_2. Addition of hexane to the CH_2Cl_2 solution precipitated colorless crystals, which were collected by filtration, washed with hexane, and dried in vacuo. Yield: 1.75 g (2.23 mmol, 90%). Anal. Calcd for $C_{53}H_{48}N_6O$: C, 81.09; H, 6.16; N, 10.71. Found: C, 80.84; H, 6.06; N, 10.66. ^{1}H NMR (500 MHz, $CDCl_3$, rt (room temperature), δ/ppm): 1.37 (s, 18 H, ^{t}Bu), 1.80 (s, 6 H, Me), 6.89 (m, 4 H, H^b or H^c), 7.29 (d, J(H−H) = 2.5 Hz, 2 H, H^f or H^g), 7.49 (d, J(H−H) = 2.5 Hz, 2 H, H^f or H^g), 7.59 (dt, J(H−H) = 2.0, 7.5 Hz, 4 H, H^b or H^c), 8.23 (d, J(H−H) = 8.0 Hz, 4 H, H^a or H^d), 8.33 (m, 8 H, H^e and H^a or H^d).

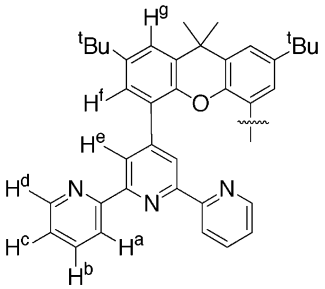

btpyxa

[(PtCl)(btpyxa)]$^+$ ([1]$^+$). Method A: Synthesis of [(PtCl)(btpyxa)](OTf). An acetonitrile solution (10 mL) of $PtCl_2(PhCN)_2$ (91.3 mg, 0.193 mmol) and AgOTf (49.7 mg, 0.193 mmol) was refluxed with stirring for 16 h under N_2. After AgCl precipitated and was removed by filtration, 1 equiv of btpyxa (152.8 mg, 0.195 mmol) was added to the filtrate under N_2. The mixture was heated at 80 °C for 3 days, and the resulting yellow precipitate was filtered off. The crude product thus obtained was washed with diethyl ether to remove unreacted btpyxa and dried in vacuo. Yield: 152.7 mg (0.131 mmol, 68%). Anal. Calcd for $C_{54}H_{48}ClF_3N_6O_4PtS\cdot 2H_2O$: C, 54.02; H, 4.37; N, 7.00. Found: C, 53.91; H, 4.25; N, 6.84. ^{1}H NMR (500 MHz, $CDCl_3$, rt, δ/ppm): 1.38 (s, 9 H, ^{t}Bu), 1.47 (s, 9 H, ^{t}Bu), 1.84 (s, 6 H, Me), 6.93 (dd, J(H−H) = 5.5, 6.5 Hz, 2 H, tpy), 7.28 (m, obscured by $CHCl_3$, xanthene and trpy), 7.56 (d, J(H−H) = 2.5 Hz, 1 H, xanthene), 7.64 (d, J(H−H) = 2.5 Hz, 1 H, xanthene), 7.68 (d, J(H−H) = 2.5 Hz, 1 H, xanthene), 7.73 (t, J(H−H) = 7.0 Hz, 2 H, trpy), 7.86 (t, J(H−H) = 8.0 Hz, 2 H, trpy), 7.96 (d, J(H−H) = 8.0 Hz, 2 H, trpy), 8.15 (s, 2 H, trpy), 8.30 (d, 2 H, trpy), 8.36 (d, J(H−H) = 8.5 Hz, 2 H, trpy), 8.38 (s, 2 H, trpy), 8.68 (d, J(H−H) = 5.5 Hz, 2 H, trpy). ESI-MS: *m*/*z* 1015 ([(PtCl)(btpyxa)]$^+$). Electronic absorption data (CH_2Cl_2 solution): λ_{max} 391 nm (ϵ 4300 M^{-1} cm^{-1}), 416 nm (ϵ 4900 M^{-1} cm^{-1}).

Method B: Synthesis of [(PtCl)(btpyxa)](PF$_6$). A mixture of $PtCl_2$(cod) (193.0 mg, 0.516 mmol) and btpyxa (404.8 mg, 0.516 mmol) suspended in methanol (80 mL) was deoxygenated by bubbling N_2 through it for 75 min and was then stirred at 50 °C for 3 h. The resulting yellow solution was filtered to remove any $PtCl_2$(cod) and btpyxa that remained unreacted. Addition of a saturated aqueous solution of NH_4PF_6 to the filtrate precipitated yellow microcrystals, which were separated by filtration, washed with water and then diethyl ether, and dried in vacuo. Yield: 575.2 mg (0.496 mmol, 96%). Anal. Calcd for $C_{53}H_{48}ClF_6N_6OPPt\cdot 3H_2O$: C, 52.41; H, 4.48; N, 6.92. Found: C, 52.63; H, 4.23; N, 6.89.

[(PtCl)$_2$(btpyxa)](PF$_6$)$_2$ ([2](PF$_6$)$_2$). A methanol suspension (40 mL) of $PtCl_2$(cod) (98.0 mg, 0.262 mmol) and btpyxa (68.5 mg, 0.087 mmol) was warmed at 70 °C for 19 h under N_2. The resulting yellow solution was filtered to remove unreacted $PtCl_2$(cod). Addition of a saturated aqueous solution of NH_4PF_6 to the filtrate precipitated yellow solids, which were separated by filtration, washed with water and then diethyl ether, and dried in vacuo. Yield: 123.9 mg (0.081 mmol, 92%). Anal. Calcd for $C_{53}H_{48}Cl_2F_{12}N_6OP_2Pt_2\cdot H_2O$: C, 40.96; H, 3.24; N, 5.41. Found: C, 41.00; H, 3.36; N, 5.44. ^{1}H NMR (500 MHz, CD_3CN, rt, δ/ppm): 1.41 (s, 18 H, ^{t}Bu), 1.87 (s, 6 H, Me), 7.52 (d, J(H−H) = 2.5 Hz, 2 H, xanthene), 7.63 (t, J(H−H) = 5.9 Hz, 4 H, trpy), 7.86 (d, J(H−H) = 2.5 Hz, 2 H, xanthene), 7.96 (t, J(H−H) = 7.8 Hz, 4 H, trpy), 8.01 (t, J(H−H) = 7.8 Hz, 4 H, trpy), 8.26 (s, 4 H, trpy), 9.06 (d, J(H−H) = 5.4 Hz, 4 H, trpy). ESI-MS: *m*/*z* 623 ([(PtCl)$_2$(btpyxa)]$^{2+}$). Electronic absorption data (CH_3CN solution): λ_{max} 421 nm (ϵ 10 000 M^{-1} cm^{-1}).

[(PtCl){RuCl$_2$(dmso)}(btpyxa)](PF$_6$) ([3](PF$_6$)). A mixture of [**1**](PF$_6$) (410.2 mg, 0.353 mmol) and $RuCl_2(dmso)_4$ (171.2 mg, 0.353 mmol) suspended in ethanol (80 mL) was refluxed with stirring for 2 days under N_2. The reddish brown solid which precipitated was separated by centrifugation. The product thus obtained was washed with acetone and dried in vacuo. Yield: 412.5 mg (0.292 mmol, 83%). Anal. Calcd for $C_{55}H_{54}Cl_3F_6N_6O_2PPtRuS\cdot H_2O$: C, 46.24; H, 3.95; N, 5.88. Found: C, 46.09; H, 4.00; N, 5.84. ESI-MS: *m*/*z* 615 ([(PtCl){RuCl(dmso)}(btpyxa)]$^{2+}$). IR (KBr): 1102 cm^{-1} (ν_{SO}).

[(PtCl){Ru(^{t}Bu$_2$SQ)(dmso)}(btpyxa)](PF$_6$)$_2$ ([4](PF$_6$)$_2$). A methanolic solution (15 mL) of potassium *tert*-butoxide (8.32 mg, 0.0741 mmol) was added to 3,5-di-*tert*-butylcatechol (8.24 mg, 0.0371 mmol) in the same solvent (20 mL), and the mixture was stirred for 30 min under N_2. The solution was added to a methanolic suspension (100 mL) of [**3**](PF$_6$) (52.3 mg, 0.0371 mmol), and then the mixture was stirred at 50 °C for 14 h. The resulting green solution was evaporated to dryness under reduced pressure. The residue was dissolved in a small amount of acetone and purified by column chromatography using an alumina A-Super I column (ICN Biomedicals GmbH). A green band of [**4**]$^{2+}$ eluted with acetone was collected by filtration and dried under reduced pressure. The residue was extracted with methanol. Addition of a saturated aqueous solution of NH_4PF_6 to the methanol solution resulted in precipitation of a green solid, which was separated by centrifugation, washed with water, and dried in vacuo. Yield: 29.3 mg (0.0172 mmol, 46%). Anal. Calcd for $C_{69}H_{74}ClF_{12}N_6O_4P_2PtRuS\cdot 3H_2O$: C, 47.11; H, 4.58; N, 4.78. Found: C, 47.24; H, 4.32; N, 4.90. ESI-

(7) (a) Constable, E. C.; Ward, M. D. *J. Chem. Soc., Dalton Trans.* **1990**, 1405−1409. (b) Potts, K. T.; Konwar, D. *J. Org. Chem.*, **1991**, *56*, 4815−4816.
(8) Aikawa, K.; Nagata, T. *Inorg. Chim. Acta* **2000**, *306*, 223−226.
(9) Braunstein, P.; Bender, R.; Jud, J. *Inorg. Synth.* **1987**, *26*, 341−350.
(10) McDermott, J. X.; White, J. F.; Whitesides, G. M. *J. Am. Chem. Soc.* **1976**, *98*, 6521−6528.
(11) Evans, I. P.; Spencer, A.; Wilkinson, G. *J. Chem. Soc., Dalton Trans.* **1973**, 204−209.
(12) Norrby, T.; Börje, A.; Åkermark, B.; Hammarstorm, L.; Alsins, J.; Lashgari, K.; Norrestam, R.; Mårtensson, J.; Stenhagen, G. *Inorg. Chem.* **1997**, *36*, 5850−5858.

MS: *m*/*z* 708 ([(PtCl){Ru(ᵗBu$_2$SQ)(dmso)}(btpyxa)]$^{2+}$), 669 ([**4**]$^{2+}$ − dmso). Electronic absorption data (CH_2Cl_2 solution): λ_{max} 273 nm (ϵ 52 200 M^{-1} cm^{-1}), 284 nm (ϵ 52 300 M^{-1} cm^{-1}), 308 nm (ϵ 43 500 M^{-1} cm^{-1}), 421 nm (ϵ 8100 M^{-1} cm^{-1}), 742 nm (ϵ 6200 M^{-1} cm^{-1}). EPR (CH_2Cl_2, 293 K): $g = 2.00$, $G = 0.69$ mT. IR (KBr): 1095 cm^{-1} (ν_{SO}).

[Ru(ᵗBu$_2$SQ)(dmso)(trpy)](PF$_6$) ([5](PF$_6$)). A methanolic solution (15 mL) of potassium *tert*-butoxide (45.5 mg, 0.405 mmol) was mixed with 3,5-di-*tert*-butylcatechol (45.1 mg, 0.203 mmol) in the same solvent (15 mL), and the solution was stirred for 30 min under N_2. The solution was added to $RuCl_2$(dmso)(trpy) (98.1 mg, 0.203 mmol) suspended in methanol (50 mL) and stirred at 50 °C for 27 h. The resulting green solution was evaporated to dryness. The residue was dissolved in a small amount of acetone and purified by column chromatography using an alumina A-Super I column (ICN Biomedicals GmbH). A green band of [**5**]$^+$ eluted with acetone/MeOH (9:1 v/v) was collected and evaporated to dryness. The residue was extracted with methanol. Addition of a saturated aqueous solution of NH_4PF_6 to the solution precipitated a green solid, which was separated by centrifugation, washed with water, and dried in vacuo. Yield: 105.6 mg (0.138 mmol, 67%). Anal. Calcd for $C_{31}H_{37}F_6N_3O_3PRuS$: C, 47.87; H, 4.80; N, 5.40. Found: C, 47.59; H, 4.87; N, 5.43. ESI-MS: *m*/*z* 633 ([Ru(ᵗBu$_2$SQ)(dmso)(trpy)]$^+$). Electronic absorption data (CH_2Cl_2 solution): λ_{max} 271 nm (ϵ 24 100 M^{-1} cm^{-1}), 308 nm (ϵ 35 400 M^{-1} cm^{-1}), 457 nm (ϵ 5100 M^{-1} cm^{-1}), 737 nm (ϵ 7500 M^{-1} cm^{-1}). EPR (CH_2Cl_2, 293 K): $g = 2.00$, $G = 0.63$ mT. IR (KBr): 1099 cm^{-1} (ν_{SO}).

Physical Measurements. ^{1}H NMR was performed with a JEOL GX-500 spectrometer. ESI-MS spectra were measured with a Shimadzu LCMS-2010 liquid chromatograph mass spectrometer. Elemental analyses were carried out at the Research Center for Molecular-Scale Nanoscience, Institute for Molecular Science. Cyclic voltammetry (CV) was performed with an ALS/Chi model 660 electrochemical analyzer. Cyclic voltammograms were recorded at a scan rate of 100 mV s^{-1} at room temperature using a glassy carbon working electrode, a Pt wire counter electrode, and a Ag/$Ag(NO_3)$ (0.01 mmol dm^{-3}) reference electrode. All potentials were converted to SCE ($E_{SCE} = E_{Ag/Ag^+} + 0.327$ V). Spectroelectrochemical measurements of UV−vis−NIR spectra were conducted using a thin-layer electrode cell with a platinum minigrid working electrode sandwiched between the two glass sides of an optical cell (path length 0.5 mm), a platinum counter electrode, and an Ag/$Ag(NO_3)$ reference electrode. A Hokuto Denko HA-501 potentiostat and a Shimadzu UV-3100PC UV−vis−NIR scanning spectrophotometer were used. EPR spectra were measured with a JEOL X-band spectrometer (JES-RE1XE). The *g* values were calibrated precisely with an Mn^{2+} marker.

X-ray Crystallography. Yellow crystals of [**1**](PF$_6$)·$CHCl_3$ were obtained by vapor diffusion of diethyl ether into a chloroform solution of the complex. Brown crystals of [**5**](PF$_6$) were obtained by slow evaporation of a methanol−water solution of the complex. The crystal data for [**1**](PF$_6$)·$CHCl_3$ and [**5**](PF$_6$) are summarized in Table 1.

Data for [**1**](PF$_6$)·$CHCl_3$ and [**5**](PF$_6$) were collected on a Rigaku/MSC Mercury CCD diffractometer using graphite-monochromated Mo Kα radiation ($\lambda = 0.710\ 70$ Å) at 173 K and processed using Crystal Clear.[13] The structures were solved by direct methods (SIR92)[14] and refined by full-matrix least-squares refinement on F^2. All non-hydrogen atoms were refined anisotropically. All hydrogen atoms were located in the calculated positions and not refined. All calculations were performed using the teXsan crystallographic software package.[15]

Additional information regarding the X-ray crystallography of [**2**](PF$_6$)$_2$·$6CH_3CN$ is given in the Supporting Information.

Table 1. Crystallographic Data for Complexes [**1**](PF$_6$)·$CHCl_3$ and [**5**](PF$_6$)

	[**1**](PF$_6$)·$CHCl_3$	[**5**](PF$_6$)
formula	$C_{53}H_{48}ClF_6N_6OPPt$·$CHCl_3$	$C_{31}H_{37}F_6N_3O_3PRuS$
fw	1279.89	777.75
color	yellow	brown
cryst size/mm^3	0.25 × 0.15 × 0.05	0.25 × 0.03 × 0.03
cryst system	triclinic	triclinic
space group	$P\bar{1}$	$P\bar{1}$
a/Å	14.125(3)	8.972(4)
b/Å	14.833(3)	12.609(5)
c/Å	15.718(3)	15.791(6)
α/deg	63.540(8)	70.94(1)
β/deg	68.387(8)	73.23(1)
γ/deg	76.382(8)	82.10(2)
V/Å^3	2730.7(9)	1614(1)
Z	2	2
T/K	−173	−173
D_{calc}/g cm^{-3}	1.557	1.599
radiatn (λ/Å)	Mo Kα (0.710 70)	Mo Kα (0.710 70)
μ/cm^{-1}	28.48	6.72
F(000)	1276.00	794.00
$2\theta_{max}$/deg	55.0	55.0
no. of reflcns (all, $2\theta < 54.97°$)	11 963	7123
no. of variables	651	410
reflcn/param ratio	18.38	17.16
GOF	2.33	1.05
R1[a] [$I > 2\sigma(I)$]	0.063	0.070
R^b (all data)	0.109	0.115
R_w^c (all data)	0.186	0.138

[a] $R1 = \Sigma||F_o^2| - |F_c^2||/\Sigma|F_o^2|$. [b] $R = \Sigma(F_o^2 - F_c^2)/\Sigma F_o^2$. [c] $R_w = [(\Sigma w(F_o^2 - F_c^2)^2/\Sigma w(F_o^2)^2)]^{1/2}$.

Results and Discussion

Ligand Synthesis. Previously, we reported dinuclear Ru−dioxolene complexes bridged by 1,8-bis(2,2′:6′,2″-terpyridyl)anthracene.[5] Here, we have used a xanthene moiety to bridge two metal−terpyridyl groups to increase the flexibility of the bridging unit compared to the previous anthracene moiety. A new bridging ligand, btpyxa, was synthesized as shown in Scheme 1. To incorporate two terpyridyl groups into xanthene, 2,7-di-*tert*-butyl-9,9-dimethylxanthene-4,5-diboronic acid (**D**) and terpyridin-4′-yl triflate (**C**) were synthesized. Suzuki coupling between **D** and 2 equiv of **C** smoothly proceeded to give btpyxa in 90% yield. The two methyl and two *tert*-butyl groups of btpyxa were observed as magnetically equivalent signals in the ^{1}H NMR spectrum in $CDCl_3$. All of the aromatic proton signals were assigned by the ^{1}H−^{1}H COSY experiment, which also revealed the magnetic equivalency of the two terpyridyl groups of btpyxa. Thus, btpyxa has a symmetrical structure in solution.

Synthesis and Characterization of Platinum Complexes. There are two pathways to build a Pt−Ru dinuclear complex bridged by btpyxa. We first introduced platinum into the ligand to avoid the formation of the homodinuclear Ru_2-

(13) *Crystal Clear: Software Package*; Rigaku and Molecular Structure Corp: The Woodlands, TX, 1999.
(14) SIR92: Altomare, A.; Cascarano, M.; Giacovazzo, C.; Guagliardi, A. *J. Appl. Crystallogr.* **1993**, *26*, 343−350.
(15) *teXsan: Crystal Structure Analysis Package*; Molecular Structure Corp: The Woodlands, TX, 1985, 1999.

Scheme 1. Synthesis of the btpyxa Ligand

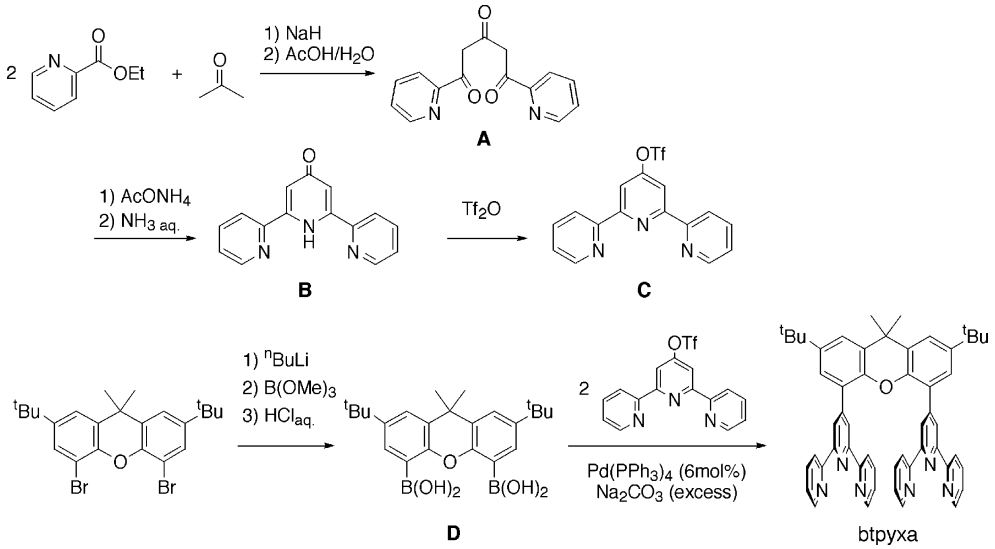

(btpyxa) framework due to the strong affinity of ruthenium(II) for terpyridyl. Treatment of $PtCl_2(PhCN)_2$ with AgOTf in CH_3CN and the subsequent reaction with btpyxa at 100 °C for 24 h in MeCN gave a ca. 3:1 mixture of $[(PtCl)(btpyxa)]^+$ ($[\mathbf{1}]^+$) and $[(PtCl)_2(btpyxa)]^{2+}$ ($[\mathbf{2}]^{2+}$) (total yield 80%). The same reaction conducted at 80 °C for 3 days selectively produced the monomer complex [(PtCl)(btpyxa)](OTf) ([**1**](OTf)) in 70% yield (eq 1).

$$PtCl_2(PhCN)_2 \xrightarrow[2)\ btpyxa]{1)\ AgOTf} [(PtCl)(btpyxa)](OTf) \quad (1)$$

[1](OTf)

Moreover, $[\mathbf{1}]^+$ was obtained in almost quantitative yield by the reaction of $PtCl_2$(cod) with 1 equiv of btpyxa in MeOH at 50 °C for 3 h (eq 2).

$$\text{btpyxa} \xrightarrow[\text{MeOH, 50 °C, 3 h}]{PtCl_2(cod)\ (1\ eq.)} \xrightarrow{NH_4PF_6} [(PtCl)(btpyxa)](PF_6) \quad (2)$$

[1](PF$_6$)

We also synthesized $[\mathbf{2}]^{2+}$ in 92% yield by treating btpyxa with an excess of $PtCl_2$(cod) at 70 °C for 19 h (eq 3).

$$\text{btpyxa} \xrightarrow[\text{MeOH, 70 °C, 17 h}]{PtCl_2(cod)\ (3\ eq.)} \xrightarrow{NH_4PF_6} [(PtCl)_2(btpyxa)](PF_6)_2 \quad (3)$$

[2](PF$_6$)$_2$

The ESI-MS (electrospray ionization mass) spectra of $[\mathbf{1}]^+$ and $[\mathbf{2}]^{2+}$ in MeCN exhibited parent peaks at *m*/*z* 1015 and 623 for $[(PtCl)(btpyxa)]^+$ and $[(PtCl)_2(btpyxa)]^{2+}$, respectively. The ^{1}H NMR spectra of [**1**](OTf) in $CDCl_3$ displayed two *tert*-butyl and 13 aromatic proton signals (total 24 protons) due to the asymmetrical structure of $[\mathbf{1}]^+$. On the other hand, the two methyl, two *tert*-butyl, and two terpyridyl groups of the btpyxa ligand appeared as magnetically equivalent signals in the ^{1}H NMR of $[\mathbf{2}]^{2+}$ in CD_3CN. The electronic absorption spectrum of [**1**](OTf) in CH_2Cl_2 showed two bands at 416 nm (ϵ 4900 M^{-1} cm^{-1}) and 391 nm (ϵ 4300 M^{-1} cm^{-1}) in the visible region. These bands are attributed to metal-to-ligand charge transfer (MLCT) transitions by analogy with the electronic spectrum of [(PtCl)(R-trpy)]$^+$ (R-trpy denotes 2,2′:6′,2″-terpyridine and terpyridines with substituents at the 4′-position).[16] In fact, $[\mathbf{2}]^{2+}$ also displayed a band at 421 nm with an almost 2-fold molecular extinction coefficient (ϵ 10 000 M^{-1} cm^{-1}) compared with that of $[\mathbf{1}]^+$.

The cyclic voltammogram (CV) of [1](PF_6) in DMSO exhibits two reversible redox waves at $E_{1/2} = -0.94$ V and -1.50 V versus SCE,[17] which are quite close to those of [(PtX)(R-trpy)]$^+$ (X denotes a substituent group).[16d,h,18] In the CV of [**2**](PF_6)$_2$ in DMSO, the reversible redox couples of $[\mathbf{1}]^+$ at $E_{1/2} = -0.94$ and -1.50 V split into two redox couples at $E_{1/2} = -0.80$ and -0.96 V and $E_{1/2} = -1.48$ and -1.59 V, respectively, suggesting electronic interaction between the two Pt(trpy) groups. The pattern and redox potential for the CV of $[\mathbf{2}]^{2+}$ were independent of the concentration of the complex (0.1−1.0 mM). In addition, such interaction was not observed at all in the CV of $[\mathbf{1}]^+$. The appearance of the four redox couples in the CV of $[\mathbf{2}]^{2+}$, therefore, is attributable to intramolecular interaction between two Pt(trpy) groups rather than an intermolecular one.

Crystal Structure of [1](PF$_6$)·CHCl$_3$. The molecular structure of [**1**](PF_6)·$CHCl_3$ was determined by X-ray

(16) (a) Yip, H.-K.; Cheng, L.-K.; Cheung, K.-K.; Che, C.-M. *J. Chem. Soc., Dalton Trans.* **1993**, 2933−2938. (b) Aldridge, T. K.; Stacy, E. M.; McMillin, D. R. *Inorg. Chem.* **1994**, *33*, 722−727. (c) Bailey, J. A.; Hill, M. G.; Marsh, R. E.; Miskowski, V. M.; Schaefer, W. P.; Gray, H. B. *Inorg. Chem.* **1995**, *34*, 4591−4599. (d) Crites, D. K.; Cunningham, C. T.; McMillin, D. R. *Inorg. Chim. Acta* **1998**, *273*, 346−353. (e) Arena, G.; Calogero, G.; Campagna, S.; Scolaro, L. M.; Ricevuto, V.; Romeo, R. *Inorg. Chem.* **1998**, *37*, 2763−2769. (f) Büchner, R.; Cunningham, C. T.; Field, J. S.; Haines, R. J.; McMillin, D. R.; Summerton, G. C. *J. Chem. Soc., Dalton Trans.* **1999**, 711−717. (g) Lai, S.-W.; Chan, M. C. W.; Cheung, K.-K.; Che, C.-M. *Inorg. Chem.* **1999**, *38*, 4262−4267. (h) Michalec, J. F.; Bejune, S. A.; Cuttell, D. G.; Summerton, G. C.; Gertenbach, J. A.; Field, J. S.; Haines, R. J.; McMillin, D. R. *Inorg. Chem.* **2001**, *40*, 2193−2200.

(17) In the case of CV of [**1**](OTf) using CH_2Cl_2, the first reduction peak was observed at $E_{1/2} = -0.78$ V and the second reduction was not observed due to limited potential window.

Table 2. Selected Bond Lengths (Å) and Bond Angles (deg) of [**1**](PF_6)·$CHCl_3$[a]

Pt1−Cl1	2.294(2)	Pt1−N1	2.036(7)
Pt1−N2	1.945(6)	Pt1−N3	2.016(7)
Cl1−Pt1−N1	98.3(2)	N1−Pt1−N2	81.7(3)
Cl1−Pt1−N3	99.3(2)	N2−Pt1−N3	80.8(3)

[a] Intramolecular distances: N2···N5, 4.12 Å; C8···C23, 4.42 Å; C34···C35, 4.66 Å. Intermolecular distance: Pt···Pt, 3.42 Å.

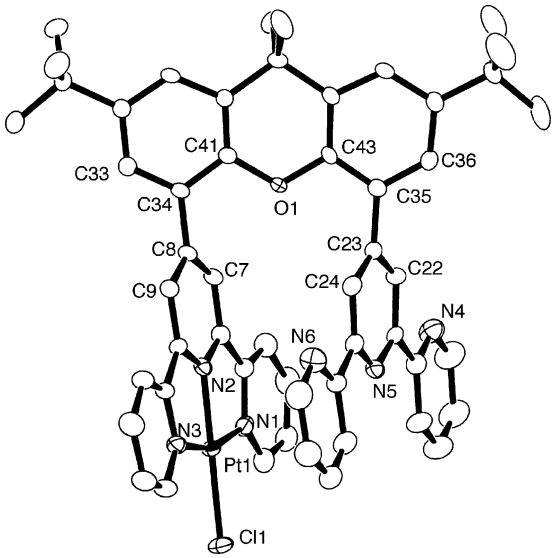

Figure 1. ORTEP drawing of the cationic part of [**1**](PF_6)·$CHCl_3$ with 50% thermal ellipsoids. Hydrogen atoms are omitted for clarity.

crystallographic analysis. Selected bond lengths and bond angles are presented in Table 2, and the ORTEP drawing of the cation part of [**1**](PF_6)·$CHCl_3$ is shown in Figure 1.

One terpyridine unit in btpyxa chelates a platinum atom whose coordination geometry is square planar, and the other unit is free. The Pt−N distances are comparable to those of platinum−terpyridine and substituted-terpyridine complexes, and the distance between Pt and the inner N atom (Pt1−N2, 1.945(6) Å) is significantly shorter than those of the two outer N atoms (Pt1−N1, 2.036(7) Å; Pt1−N3, 2.016(7) Å). The xanthene framework is almost flat. Two terpyridine units are located nearly in parallel, since the dihedral angles of the xanthene plane and the center pyridine ring of terpyridine linked to PtCl and that of the metal-free site are −55.3° (average) (C7−C8−C34−C41 = −54.4(9)° and C9−C8−C34−C33 = −56.1(10)°) and −59.5° (average) (C22−C23−C35−C36 = −55.9(10)° and C24−C23−C35−C43 = −63.1(10)°), respectively. Intramolecular atomic distances between C34 and C35, C8 and C23, and N2 and N5 are 4.66, 4.42, and 4.12 Å, respectively. On the basis of these atomic distances, the two terpyridines planes may be too far to form an intramolecular $\pi-\pi$ stacking. In the crystal structure, [**1**](PF_6)·$CHCl_3$ forms head-to-head columns, in which the intermolecular Pt···Pt atomic and the closest terpyridine···terpyridine distances are 3.42 and 3.69 Å, respectively (Figure 2). The head-to-head columns of $[\mathbf{1}]^+$ are ascribed to the intermolecular $\pi-\pi$ interaction between two metal-free terpyridine planes and the $\sigma-\sigma$ one between two Pt atoms in the adjacent two complexes, as depicted in Figure 2. Indeed, the intermolecular Pt···Pt atomic distance

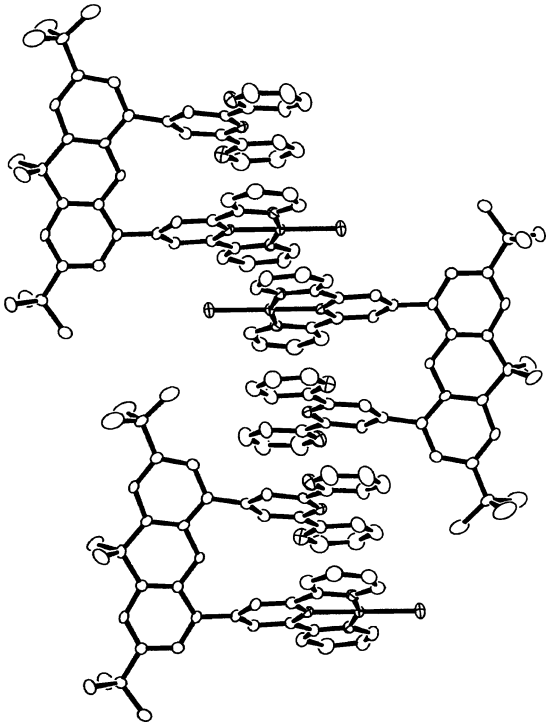

Figure 2. Crystal packing of [**1**](PF_6)·$CHCl_3$. The PF_6^- ion and $CHCl_3$ molecule are omitted for clarity.

for two adjacent $[\mathbf{1}]^+$ is quite close to that of $[(PtX)(R\text{-trpy})]^+$ stacked in zigzag columns in the solid state.[16a,c,f,g,18c,19]

The diplatinum complex [**2**](PF_6)$_2$ also formed zigzag columns with intermolecular Pt···Pt atomic distances of 4.39 and 4.20 Å in the crystal structure (Figures S1 and S2, Supporting Information).[20] The bond lengths and angles of the two [(PtCl)(trpy)] units in $[\mathbf{2}]^{2+}$ are very close to those of $[\mathbf{1}]^+$. The intramolecular Pt···Pt atomic distance of 4.38 Å would be attributable to the size of the framework of the btpyxa ligand.

Synthesis of Platinum−Ruthenium−Dioxolene Complex $[\mathbf{4}]^{2+}$. The synthesis of the platinum−ruthenium−dioxolene complex [**4**](PF_6)$_2$ is outlined in Scheme 2.

The reaction of [**1**](PF_6) with 1 equiv of $RuCl_2(dmso)_4$ in refluxing EtOH afforded [(PtCl){$RuCl_2$(dmso)}(btpyxa)](PF_6) ([**3**](PF_6)) as a reddish brown precipitate. The reaction of [**3**](PF_6) with 3,5-di-*tert*-butylcatechol in the presence of 2 equiv of ^{t}BuOK at 50 °C in MeOH produced [(PtCl){Ru(^{t}Bu$_2$SQ)(dmso)}(btpyxa)]$^{2+}$ ($[\mathbf{4}]^{2+}$), and subseqent treatment with NH_4PF_6 gave [**4**](PF_6)$_2$ as a green powder. The ESI-MS spectrum of [**4**](PF_6)$_2$ showed two dication peaks at *m*/*z* 708 and 669 assignable to [(PtCl){Ru(^{t}Bu$_2$SQ)(dmso)}-

(18) (a) Yang, L.; Wimmer, F. L.; Wimmer, S.; Zhao, J.; Braterman, P. S. *J. Organomet. Chem.* **1996**, *525*, 1−8. (b) Hill, M. G.; Bailey, J. A.; Miskowski, V. M.; Gray, H. B. *Inorg. Chem.* **1996**, *35*, 4585−4590. (c) Yam, V. W.-W.; Tang, R. P.-L.; Wong, K. M.-C.; Cheung, K.-K. *Organometallics* **2001**, *20*, 4476−4482. (d) Jude, H.; Krause Bauer, J. A.; Connick, W. B. *J. Am. Chem. Soc.* **2003**, *125*, 3446−3447.

(19) Romeo, R.; Scolaro, L. M.; Plutino, M. R.; Albinati, A. *J. Organomet. Chem.* **2000**, *593*−*594*, 403−408.

(20) The crystal structure of [**2**](PF_6)$_2$ was determined by X-ray crystallography (R1 = 6.5%), and the crystal structure of [**2**](PF_6) is shown in Figures S1 and S2 (Supporting Information). One of the carbon atoms of the terpyridine moiety was not refined anisotropically, but the intra- and intermolecular Pt···Pt atomic distances were precisiely determined.

Scheme 2. Synthesis of [**4**](PF$_6$)$_2$

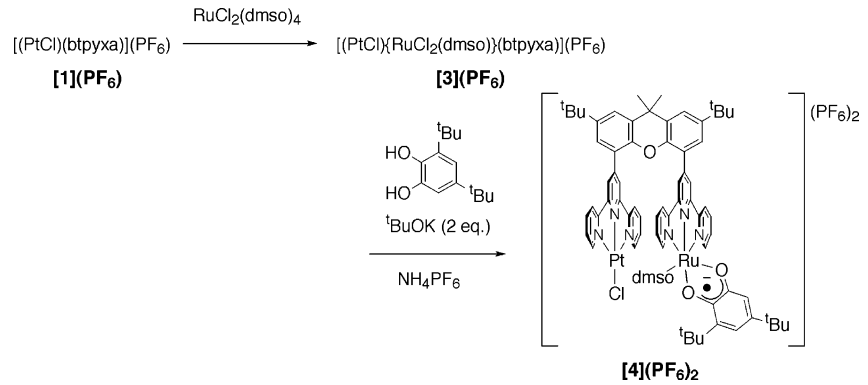

Scheme 3. Synthesis of [**5**](PF$_6$)

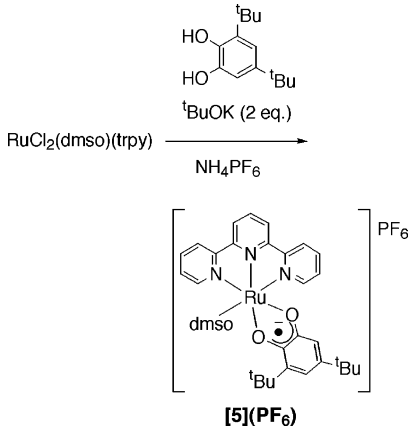

(btpyxa)]$^{2+}$ and [(PtCl){Ru(^{t}Bu$_2$SQ)}(btpyxa)]$^{2+}$, respectively. The presence of the ^{t}Bu$_2$SQ radical in [**4**](PF$_6$)$_2$ was evidenced by the appearance of a sharp signal at $g = 2.00$ with a peak to peak separation of 0.69 mT in the EPR spectrum in CH_2Cl_2 at 293 K.

Synthesis and X-ray Structure of Ruthenium−Semiquinone Complex [5](PF$_6$). To compare to [**4**](PF$_6$)$_2$, monomeric [Ru(^{t}Bu$_2$SQ)(dmso)(trpy)](PF$_6$) ([**5**](PF$_6$)) was prepared by the reaction of RuCl$_2$(dmso)(trpy) with 3,5-di-*tert*-butylcatechol in the presence of 2 equiv of ^{t}BuOK (Scheme 3).

The EPR spectrum of [**5**](PF$_6$) also displayed the signal at $g = 2.00$ attributed to the semiquinone anion radical. The X-ray structure of [**5**](PF$_6$) is shown in Figure 3, and selected bond lengths and bond angles are listed in Table 3.

Although [**5**](PF$_6$) is expected to have two isomers with regard to the orientation of the two *tert*-butyl groups of the C6 ring of the semiquinone ligand, one isomer selectively crystallized under the experimental conditions. DMSO is linked to Ru through the S atom with a bond distance of 2.232(2) Å. The two C−O bond distances in the coordinated dioxolene (C1−O1, 1.320(6) Å, and C2−O2, 1.315(6) Å) are comparable to those in a range of semiquinone forms.[2,3,4] Attempts to grow single crystals of [**4**](PF$_6$)$_2$ for X-ray analysis have not been successful. The molecular structure around the Ru atom of [**4**]$^{2+}$ would be very close to that of [**5**]$^+$ (Scheme 2) on the basis of the similarities in the CV and electronic absorption spectra between [**4**](PF$_6$)$_2$ and [**5**](PF$_6$) (vide infra). Indeed, the IR spectra of [**4**](PF$_6$)$_2$ and

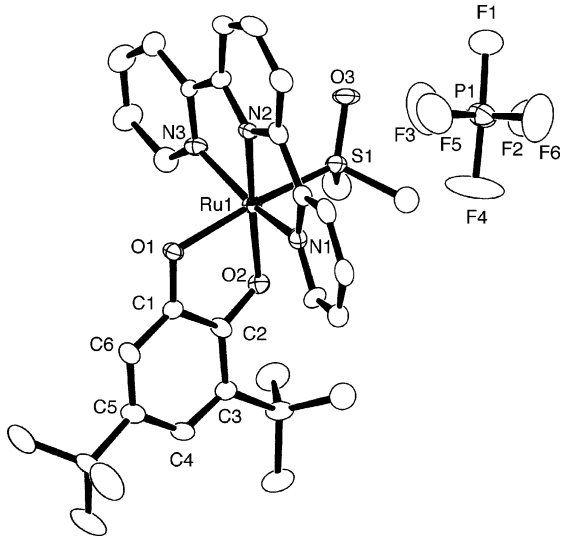

Figure 3. ORTEP drawing of [**5**](PF$_6$) with 50% thermal ellipsoids. Hydrogen atoms are omitted for clarity.

Table 3. Selected Bond Lengths (Å) of [**5**](PF$_6$)

Ru1−N1	2.071(5)	Ru1−N2	1.979(3)
Ru1−N3	2.073(5)	Ru1−S1	2.232(2)
Ru1−O1	2.075(4)	Ru1−O2	2.039(3)
C1−O1	1.320(6)	C2−O2	1.315(6)
C1−C2	1.451(7)	C2−C3	1.413(7)
C3−C4	1.374(7)	C4−C5	1.436(8)
C5−C6	1.360(7)	C6−C1	1.405(7)
S1−O3	1.479(4)		

[**5**](PF$_6$) showed the strong ν_{SO}(*S*-bound) band at 1095 and 1099 cm^{-1}, respectively.[21]

Redox Behavior. The cyclic voltammogram (CV) of [**4**](PF$_6$)$_2$ in CH_2Cl_2 exhibits three reversible redox waves at $E_{1/2} = +0.64$, -0.33, and -0.74 V vs SCE (Figure 4A). The redox waves at $E_{1/2} = +0.64$ V and -0.33 V are assigned to the metal-centered Ru$^{II/III}$ couple and the ligand-based catecholato/semiquinone one, respectively, because those redox waves were also observed at $E_{1/2} = +0.65$ and -0.32 V in the CV of [**5**]$^+$ in CH_2Cl_2 (Figure 4B). The redox waves at $E_{1/2} = -0.74$ V of [**4**]$^{2+}$, therefore, are correlated with the [(PtCl)(trpy)]^0/[(PtCl)(trpy)]$^+$ couple. The corresponding redox couple for [**1**](OTf) appeared at $E_{1/2} = -0.78$ V.[17] These facts suggest that the redox reactions of the

(21) (a) Toma, H. E.; Alexiou, A. D. P. *Electrochim. Acta* **1993**, *38*, 975−980. (b) Ciofini, I.; Daul, C. A.; Adamo, C. *J. Phys. Chem. A* **2003**, 107, 11182−11190.

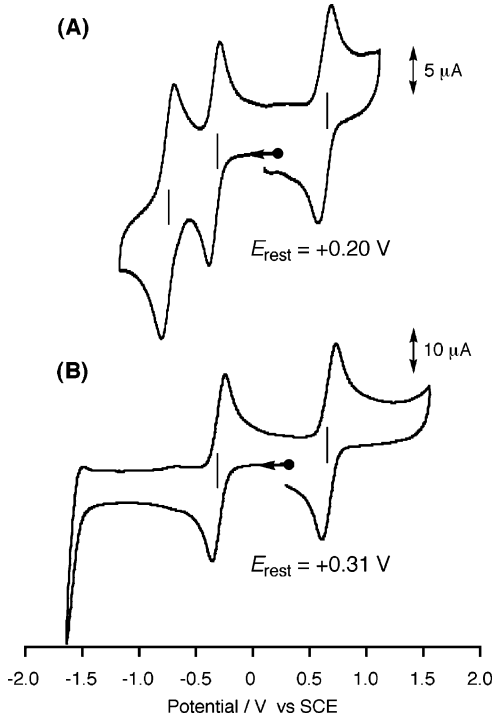

Figure 4. Cyclic voltammograms of [**4**]$(PF_6)_2$ (A) and [**5**](PF_6) (B). Conditions: 1.0 mM solution in CH_2Cl_2 containing 0.1 M $^tBu_4NPF_6$; glassy carbon working and Pt counter electrodes; scan rate 0.1 V/s; at room temperature under N_2. The arrows in the figures indicate the direction of scan.

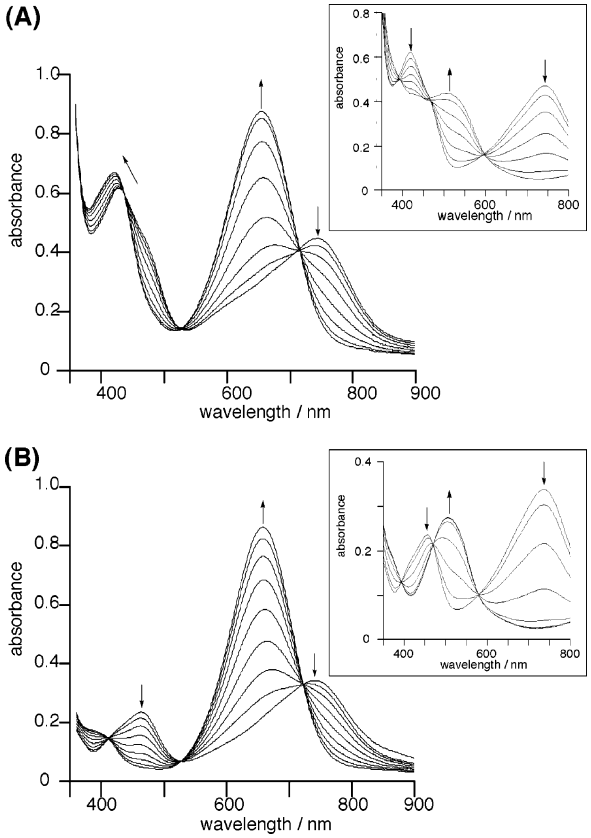

Figure 5. Absorption spectral changes during the electrochemical oxidation of [**4**]$(PF_6)_2$ (A) and [**5**](PF_6) (B) conducted at +0.93 V vs SCE. Inset: Absorption spectral changes during the electrochemical reduction of [**4**]$(PF_6)_2$ at −0.47 V and [**5**](PF_6) at −0.67 V, respectively. The arrows in the figures indicate the direction of the changes of the spectra.

[(PtCl)(trpy)] framework and the [{Ru(^{t}Bu$_2$SQ)(dmso)}-(trpy)] framework of [**4**]$^{2+}$ essentially take place independently without strong interaction with each other.

A variety of ruthenium−dmso complexes have been prepared so far. The coordination mode of dmso often varies with the oxidation state of ruthenium; dmso is usually linked to Ru^{II} with sulfur whereas it has a tendency to coordinate Ru^{III} with oxygen. As a result, redox reactions[22] and photoirradiation[23] of ruthenium−dmso complexes frequently induce linkage isomerizations of the coordinated dmso between *S*-bound and *O*-bound forms. On the other hand, Rack et al. have suggested that introduction of bidentate ligands bearing hard O-donors such as acetylacetonate and malonate to ruthenium−dmso complexes inhibits the isomerization from *S*-dmso to *O*-dmso in the oxidation of Ru^{II} to Ru^{III}.[24] In accordance with this, the CV of [**4**]$^{3+}$ that was prepared by the controlled-potential electrolysis of [**4**]$^{2+}$ at +0.97 V was same as that of [**4**]$^{2+}$. This observation ruled out the possibility of the linkage isomerization of the dmso ligand in the [**4**]$^{2+/3+}$ redox cycle. The Ru(dmso-κS) bonds of [**4**]$^{2+}$ and [**5**]$^+$, therefore, may be stabilized by the ^{t}Bu$_2$-SQ chelate. It is worthy of note that the redox potentials of [**5**]$^+$ ($E_{1/2}$ = +0.65 and −0.32 V) appeared at potentials more positive than those of [Ru(^{t}Bu$_2$SQ)(OH$_2$)(trpy)]$^{2+}$ ($E_{1/2}$ = +0.31 and −0.47 V vs SCE)[4] and [RuCl(^{t}Bu$_2$SQ)(trpy)] ($E_{1/2}$ = +0.16 and −0.73 V vs SCE).[25] Such a difference may be explained by the strong π-electron-accepting capacity of S-bonded dmso on the Ru−dioxolene framework.

Spectroelectrochemical Measurement. Ruthenium complexes having Ru^{II}−semiquinone and Ru^{III}−semiquinone frameworks usually exhibit characteristic MLCT bands (from the dπ orbital of ruthenium to the LUMO of dioxolene) around 850 and 600 nm, respectively.[3,4,26] For example, [Ru^{II}-Cl(^{t}Bu$_2$SQ)(trpy)] and [Ru^{II}(OAc)(^{t}Bu$_2$SQ)(trpy)] show strong bands at 876 nm (ϵ 19 100 M^{-1} cm^{-1}) and 883 nm (ϵ 18600 M^{-1} cm^{-1}), which shift to 592 nm (ϵ 15500 M^{-1} cm^{-1}) and 584 nm (ϵ 17 000 M^{-1} cm^{-1}), respectively, upon one electron oxidation of these complexes.[25] The absorption spectrum of [**4**]$(PF_6)_2$ in CH_2Cl_2 showed two broad bands at 742 and 421 nm that are assigned to the MLCT bands of the Ru^{II}−semiquinone and ruthenium− and/or platinum−terpyridine frameworks, respectively (Figure 5A). The mononuclear Ru complex [**5**](PF_6) also displays two strong bands at 737 and

(22) (a) Yeh, A.; Scott, N.; Taube, H. *Inorg. Chem.* **1982**, *21*, 2542−2545. (b) Silva, D. O.; Toma, H. E. *Can. J. Chem.* **1994**, *72*, 1705−1708. (c) Tomita, A.; Sano, M. *Inorg. Chem.* **1994**, *33*, 5825−5830. (d) Alessio, E.; Bolle, M.; Milani, B.; Mestroni, G.; Faleschini, P.; Geremia, S. Calligaris, M. *Inorg. Chem.* **1995**, *34*, 4716−4721.
(23) (a) Smith, M. K.; Gibson, J. A.; Young, C. G.; Broomhead, J. A.; Junk, P. C.; Keene, F. R. *Eur. J. Inorg. Chem.* **2000**, 1365−1370. (b) Rack, J. J.; Winkler, J. R.; Gray, H. B. *J. Am. Chem. Soc.* **2001**, *123*, 2432−2433. (c) Sens, C. Rodríguez, M.; Romero, I. Liobet, A. *Inorg. Chem.* **2003**, *42*, 2040−2048. (d) Rack, J. J.; Mockus, N. V. *Inorg. Chem.* **2003**, *42*, 5792−5794.
(24) Rack, J. J.; Rachford, A. A.; Shelker, A. M. *Inorg. Chem.* **2003**, *42*, 7357−7359.
(25) Kurihara, M.; Daniele, S.; Tsuge, K.; Sugimoto, H.; Tanaka, K. *Bull. Chem. Soc. Jpn.* **1998**, *71*, 867−875.
(26) Lever, A. B. P.; Masui, H.; Metcalfe, R. A.; Stufkens, D. J.; Dodsworth, E. S.; Auburn, P. R. *Coord. Chem. Rev.* **1993**, *125*, 317−331.

Scheme 4

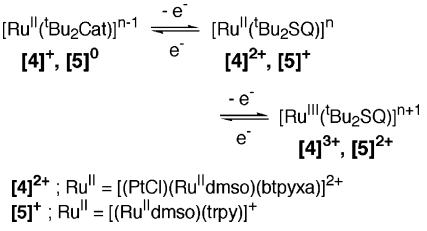

457 nm (Figure 5B). One-electron electochemical oxidation of [**4**]$(PF_6)_2$ at +0.93 V in CH_2Cl_2 resulted in the appearance of a strong band at 652 nm, and the 742 nm band of $[\mathbf{4}]^{2+}$ completely disappeared. At the same time, the band at 421 nm of $[\mathbf{4}]^{2+}$ shifted to 413 nm (Figure 5A). Similarly, the electrochemical oxidation of [**5**](PF_6) at +0.93V caused the emergence of a strong band at 654 nm with a shoulder around 400 nm, and the 737 and 457 nm bands of $[\mathbf{5}]^{+}$ disappeared (Figure 5B). When the resulting $[\mathbf{4}]^{3+}$ and $[\mathbf{5}]^{2+}$ were reduced at +0.43 V, the original absorption spectra of $[\mathbf{4}]^{2+}$ and $[\mathbf{5}]^{+}$ were fully recovered. Thus, one electron oxidation of $[\mathbf{4}]^{2+}$ and $[\mathbf{5}]^{+}$ causes a blue shift of the MLCT bands by 80−90 nm. On the other hand, the 742 nm band of $[\mathbf{4}]^{2+}$ and the 737 nm band of $[\mathbf{5}]^{+}$ completely disappeared under the controlled-potential electrolysis conditions (at −0.47 and at −0.67 V, respectively). The reoxidation of the resultant solutions at +0.43 V caused full recovery of the electronic absorption spectra of $[\mathbf{4}]^{2+}$ and $[\mathbf{5}]^{+}$. Thus, one-electron reduction of $[\mathbf{4}]^{2+}$ and $[\mathbf{5}]^{+}$ takes place in the ligand-based orbitals to form the Ru^{II}−catecholato frameworks as expressed in Scheme 4 ($^tBu_2$Cat denotes 3,5-di-*tert*-butylcatecholate ion).

The blue shift of the Ru^{II}−semiquinone MLCT band of $[\mathbf{4}]^{2+}$ (742 nm) and $[\mathbf{5}]^{+}$ (737 nm) and the red shift of the Ru^{III}−semiquinone band of $[\mathbf{4}]^{3+}$ (652 nm) and $[\mathbf{5}]^{2+}$ (654 nm) compared with those of $[Ru^{II}X(^tBu_2SQ)(trpy)]$ (X = Cl (876 nm), AcO (883 nm)) and $[Ru^{III}X(^tBu_2SQ)(trpy)]^{+}$ (X = Cl (592 nm), AcO (584 nm)) may be also attributable to the strong π-acceptor ability of S-bound dmso.

Conclusion

We have synthesized a new bridging ligand btpyxa to place two metal centers in close proximity. Mono- and diplatinum complexes $[\mathbf{1}]^{+}$ and $[\mathbf{2}]^{2+}$ were obtained by the reaction of btpyxa with 1 equiv and an excess of $PtCl_2$(cod), respectively. The X-ray structure of [**1**]$(PF_6)\cdot CHCl_3$ showed that two terpyridine units are situated in parallel. Treatment of [**1**](PF_6) with $RuCl_2(dmso)_4$ gave a platinum−ruthenium complex [**3**](PF_6). Introduction of dioxolene to the ruthenium site in $[\mathbf{3}]^{+}$ gave $[\mathbf{4}]^{2+}$. The pattern of the CV of $[\mathbf{4}]^{2+}$ was essentially the superposition of those of $[\mathbf{1}]^{+}$ and $[\mathbf{5}]^{+}$, suggesting that the redox reactions of the Pt(trpy) group and the Ru($^tBu_2$SQ) group of $[\mathbf{4}]^{2+}$ occurred independently, without strong interaction with each other. On the other hand, the CV of $[\mathbf{2}]^{2+}$ showed an electronic interaction between the two Pt(trpy) groups. Such an electronic interaction between the two Pt(trpy) moieties may be attributable to the flexibility of the xanthene unit of the btpyxa ligand in solution.

Supporting Information Available: Figures S1 and S2, displaying ORTEP drawings for [**2**]$(PF_6)_2\cdot$6MeCN, and X-ray crystallographic data for [**1**]$(PF_6)\cdot CHCl_3$, [**2**]$(PF_6)_2\cdot$6MeCN, and [**5**](PF_6) in CIF format. This material is available free of charge via the Internet at http://pubs.acs.org.

IC049680N